APL Materials

Incipient plasticity and fully plastic contact behavior of copper coated with a graphene layer

Cite as: APL Mater. **7**, 031106 (2019); https://doi.org/10.1063/1.5086333
Submitted: 20 December 2018 . Accepted: 18 February 2019 . Published Online: 12 March 2019

Sun-Young Park, Young-Cheon Kim, Rodney S. Ruoff, and Ju-Young Kim

Incipient plasticity and fully plastic contact behavior of copper coated with a graphene layer

Cite as: APL Mater. 7, 031106 (2019); doi: 10.1063/1.5086333
Submitted: 20 December 2018 • Accepted: 18 February 2019 •
Published Online: 12 March 2019

Sun-Young Park,[1,2] Young-Cheon Kim,[3] Rodney S. Ruoff,[1,4] and Ju-Young Kim[1,2,a)]

AFFILIATIONS

[1]Center for Multidimensional Carbon Materials (CMCM), Institute for Basic Science (IBS), Ulsan 44919, South Korea
[2]School of Materials Science and Engineering, UNIST (Ulsan National University of Science and Technology), Ulsan 44919, South Korea
[3]School of Advanced Materials Engineering, Andong National University, Gyeongsangbuk-do 36729, South Korea
[4]School of Natural Science, UNIST (Ulsan National University of Science and Technology), Ulsan 44919, South Korea

[a)]Author to whom correspondence should be addressed: juyoung@unist.ac.kr

ABSTRACT

Cu coated with a graphene layer increases the elastic modulus from 163.4 GPa to 176.7 GPa, as analyzed for the initial elastic loading during nanoindentation by the Hertzian contact theory. This is attributed to stiffening, due to the ultra-high elastic modulus of the graphene layer, and the compressive in-plane residual stresses in the Cu surface volume introduced by the lattice mismatch between graphene and Cu. The graphene layer induces incipient plasticity, manifested by pop-in events during nanoindentation loading, at shallower indentation depths. This could be due to the compressive in-plane residual stress in the Cu surface volume; however, this compressive stress does not significantly change the critical resolved shear stress for the incipient plasticity. Even in the fully plastic contact region, at an indentation depth of 100 nm, the graphene layer affects the stress distribution underneath the indenter, resulting in a lower pile-up height. When considering this reduced pile-up height, the graphene layer is found to enhance elastic modulus by 5%, whereas it has no effect on hardness.

Graphene exhibits remarkable mechanical properties: it has an intrinsic strength of 130 GPa and elastic modulus of 1 TPa,[1,2] as well as excellent thermal conductivity[3,4] and carrier mobility.[5] On account of these noticeable mechanical properties, many studies have been aimed at utilizing graphene as an interfacial material or surface coating material such as interlayer in composites, corrosion barrier, and lubricant materials.[6–8] Metal-graphene nanolayered composites exhibit improved compressive strength because graphene layers effectively block dislocation propagation across the metal–graphene interfaces 6. In metallic glass-graphene nanolaminates, graphene layers enhance the elastic modulus of the nanolaminates.[7] Furthermore, a considerable number of studies have investigated physical contact on the surface of graphene-coated materials because (1) physical contact with other materials is inevitable when the graphene coating is exposed, and (2) the graphene coating significantly changes the contact behavior, even though the thickness of graphene (0.34 nm) is much shallower than the contact depth.[9–11] Hammad *et al.*[9] performed nanoindentations on graphene-coated Cu film, which showed a higher load-bearing capacity in the elastic contact region than for pristine Cu film. They demonstrated that the stiffer response of graphene-coated Cu film originates from the frictionless contact between the diamond nanoindenter and the graphene layer through finite element analysis (FEA) and molecular dynamics (MD) simulations. Klemens *et al.*[10,12] studied nanoindentation, sliding, and scratching of graphene-coated Pt surfaces using atomistic simulation and friction force microscopy experiments. They found that a graphene-coated Pt surface can endure higher loads than the pristine Pt film at a shallow indentation depth, but that graphene's protective ability is lost upon rupture of the graphene layer.

In this study, the contact behavior during nanoindentation of graphene-coated Cu is investigated; the initial elastic contact

region, the transition region from elastic to plastic deformation, and the fully plastic contact region are analyzed. Stiffening due to the graphene coating is analyzed in the initial elastic contact region by the Hertzian elastic contact theory. Incipient plasticity in nanoindentation force–depth curves is observed in the form of pop-in events, whose distributions are found to depend on the graphene coating, whereas the critical resolved shear stress does not significantly depend on the graphene coating. Even in the fully plastic contact region (indentation depth of 100 nm), hardness and elastic modulus measured by the Oliver–Pharr method are affected by the graphene coating. The graphene coating is found to change the stress distribution resulting in reduced plastic pile-up.

Figure 1(a) gives a schematic overview of the sample preparation. Graphene was synthesized on a 2-mm-thick single-crystalline Cu substrate by chemical vapor deposition (CVD). Before the CVD process, the surface of the (111)-orientation single-crystalline Cu was prepared by mechanical polishing with a 0.25 μm colloidal silica suspension and electro-polishing in phosphoric acid (85% H_3PO_4) for 2 min. For the CVD process, the Cu surface was treated with H_2 gas at 1000 °C at a base pressure of 4 mTorr. Graphene was synthesized under a flow of CH_4 and H_2 gas for 4 min, and the furnace was cooled to room temperature under a flow of Ar gas. We used Raman spectroscopy mapping to confirm the quality and uniformity of CVD-grown graphene on the Cu substrate. Samples for Raman spectroscopy were prepared by transfer of graphene on a SiO_2 substrate. The graphene was transferred on the SiO_2 substrate for Raman spectroscopy measurements because the ratio of peak intensities depends on the substrate, and the ratio of 2D/G peak intensities of monolayered graphene is known to be approximately 2 for SiO_2 substrate. Nanoindentations were carried out on two samples, graphene-coated Cu (hereafter referred to as Gr-coated Cu), and pristine Cu (hereafter referred to as Gr-removed Cu). The Gr-removed Cu was prepared by physical removal of graphene from the Gr-coated Cu by using an adhesive tape. We measured Raman spectroscopy for an area of 10 μm × 10 μm at several different locations; no G and 2D peaks were observed indicating that graphene was removed completely by the adhesive tape. Nanoindentations were conducted using the continuous stiffness measurement (CSM) mode of Nanoindenter G200 (Keysight) with a diamond Berkovich indenter to a maximum indentation depth of 100 nm at a constant strain rate of 0.05 s^{-1}. At least 20 reproducible nanoindentation force–depth curves were obtained for each sample. Finite element analysis (FEA) was carried out using the commercial package ABAQUS (Simulia) to investigate the stress distribution in Cu during nanoindentation. The specimen was modeled with four-node axisymmetric reduced integration elements (CAX4R) with an analytical rigid shell of radius R = 50 nm for the nanoindenter and a 0.34 nm-thick Gr coating for Gr-coated Cu. The thickness and radius of the specimen were both 2 μm, which is enough to minimize the boundary effect for 100 nm deep nanoindentations. The material parameters of Cu used for FEA simulations were as follows: elastic modulus E =124 GPa, yield strength σ_y = 46.6 MPa, ultimate tensile strength σ_u = 217.6 MPa, and strain-hardening exponent n = 0.411 for Cu.[13] E = 1 TPa for graphene was used for FEA simulations.[2,14]

Figure 1(b) shows that the 2D/G peak intensity ratio from Raman spectroscopy is approximately two for the mapping area which is a typical feature of monolayer graphene.[15] Single-crystalline Cu with a (111)-orientation surface was found to have a polycrystalline surface after the CVD process, as shown in the electron backscatter diffraction (EBSD) image in Fig. 1(c). This polycrystallization is likely to be attributable to the dynamic nature of the Cu surface, due to sublimation and surface pre-melting, during the CVD process.[16,17] We carried out nanoindentations on surfaces with root mean squares of surface roughness R_q lower than 2 nm,[18,19] shown in yellow in the EBSD inverse pole figure map in Fig. 1(c). This surface has a misorientation angle of 23° with respect to the (100) direction of Cu. Nanoindentations for both Gr-coated and Gr-removed samples were carried out only for the surface with this crystallographic orientation for comparison. We observed reproducible nanoindentation force-depth curves for each case, and Figs. 2(a) and 2(b) show typical nanoindentation force–depth curves and the average force at every 10 nm of nanoindentation depth for Gr-coated and Gr-removed Cu. These figures show that we investigate how the graphene layer affects contact behavior in (1) the initial contact region and (2) the fully plastic contact region in the following parts.

To investigate the effect of the graphene layer on the initial elastic contact behavior during nanoindentation, typical nanoindentation force–depth curves and the distribution of indentation depth

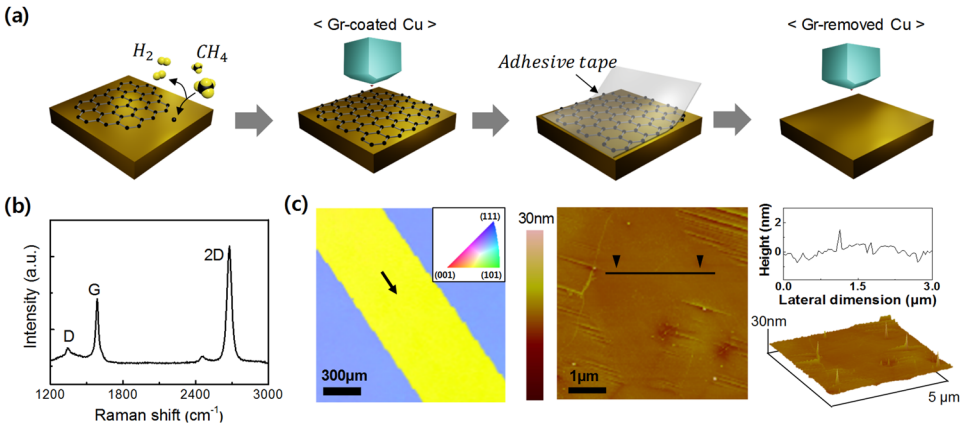

FIG. 1. (a) Schematics for sample preparations for nanoindentations. (b) Typical Raman spectra and mapping image of CVD-grown graphene. (c) Typical EBSD and AFM images of graphene-coated Cu. In yellow surfaces indicated as black arrow, nanoindentations were carried out.

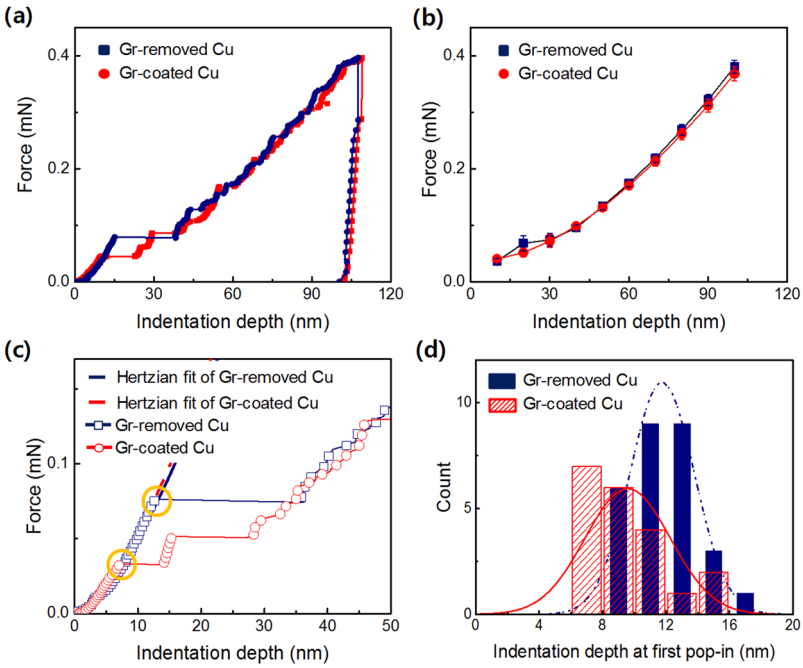

FIG. 2. (a) Typical and (b) averaged nanoindentation force-depth curves of graphene-coated Cu and graphene-removed Cu. (c) Typical nanoindentation force-indentation depth curves magnified for initial contact area. Dotted lines are Hertzian equations fitted to loading curves. (d) Histograms of indentation depth at first pop-in event of graphene-coated and graphene-removed Cu.

at the first pop-in event are presented in Figs. 2(c) and 2(d), respectively. Figure 2(c) is the enlarged graphs of Fig. 2(a) showing initial elastic loading and pop-in events better. In Fig. 2(c), Gr-coated Cu shows slightly stiffer loading than that of Gr-removed Cu. The initial elastic contact during nanoindentation can be described by the Hertzian contact theory for purely elastic contact of a sphere on a flat surface, which is given by[20–23]

$$F = \frac{4}{3}E^*\sqrt{R}h^{1.5}, \tag{1}$$

where F is the indentation force, E^* is the reduced elastic modulus, R is the radius of the indenter, and h is the indentation depth. Before the first pop-in event, for R = 50 nm (measured by observing side views of the nanoindenter in SEM), the reduced elastic moduli of Gr-removed and Gr-coated Cu were determined as 158.6 ± 17.8 GPa and 170.2 ± 17.0 GPa, respectively. In reduced elastic modulus, the effect of elastic deformation of the diamond indenter is included. By applying the relation, $1/E^* = (1 - \nu_i^2)/E_i + (1 - \nu_{mat}{}^2)/E_{mat}$ with E_i of 1141 GPa and ν_i of 0.07 for the diamond indenter, the elastic modulus of target materials can be evaluated. The elastic modulus is 163.4 ± 22.8 GPa for Gr-removed Cu and 176.7 ± 20.8 GPa for Gr-coated Cu, respectively.[24] The graphene layer, with its ultra-high elastic modulus of 1 TPa, is likely to enhance the elastic moduli only for indentation depths up to the first pop-in event (about 10 nm). Another possible reason for different stiffness is that residual stresses are induced in Cu by the lattice mismatch between graphene and Cu.[25,26] The stiffer loading curve in Gr-coated Cu could be caused by compressive in-plane residual stresses in the Cu substrate because compressive in-plane stresses act to "push" the indenter, resulting in a stiffer nanoindentation loading curve.[27]

In previous MD simulations, the compressive in-plane stress in Cu was found to decrease the critical indentation depth at which incipient plasticity occurs, whereas tensile stresses do not affect the critical indentation depth.[28] Atom clusters with severe lattice distortions, which are regarded as precursors for the nucleation of dislocations, were formed beneath the indenter before the critical indentation depth due to shear stress. At the critical indentation depth, the shear stress applied on these clusters exceeds the critical resolved shear stress, and thus, dislocations nucleate, extending on (111) slip planes. The critical indentation depth corresponds to the indentation depth at the first pop-in event. Figure 2(d) shows a histogram of indentation depth at the first pop-in event for all measurements of Gr-removed and Gr-coated Cu. The indentation depth at the first pop-in event for Gr-coated Cu is shallower than that for Gr-removed Cu, which indicates that compressive in-plane residual stresses might be introduced to the top surface volume of the Cu due to the graphene coating, which agrees with the presumption that compressive stress stiffens the initial elastic loading curves for Gr-coated Cu. The critical resolved shear stress applied on these dislocation precursors, τ_{max}, can be described by[20–22,29]

$$\tau_{max} = 0.31\left(\frac{6FE^{*2}}{\pi^3R^2}\right)^{1/3}, \tag{2}$$

where F is the indentation force at the indentation depth of the first pop-in event. With an estimated indenter radius R = 50 nm, the critical resolved shear stress was found to be 15.5 ± 0.98 GPa for Gr-removed Cu and 14.4 ± 1.11 GPa for Gr-coated Cu. The difference in the critical resolved shear stress between the two samples is smaller than for the indentation depths of the first pop-in events, and the values are similar to the theoretical shear strength of Cu (15 GPa) calculated by $\mu_s/2\pi$.[22,30] Despite the thickness of graphene (0.34 nm), the graphene coating affects both the

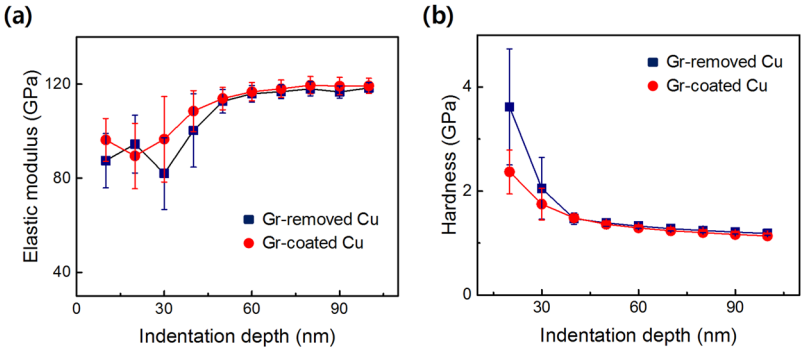

FIG. 3. (a) Averaged elastic modulus and (b) hardness of graphene-coated and graphene-removed Cu measured by the Oliver-Pharr method.

initial elastic loading and incipient plasticity as described above, possibly because the graphene layer has an ultra-high elastic modulus and introduces compressive in-plane residual stress in Cu.

We investigate how graphene coating affects the measured mechanical properties for fully plastic contact region at greater indentation depths. The average elastic modulus and hardness at every 10 nm of indentation depth were measured by the Oliver–Pharr method,[24,31] as shown in Figs. 3(a) and 3(b), respectively. The elastic modulus converged for indentation depths deeper than about 60 nm. At the maximum indentation depth (100 nm), an elastic modulus of 117.4 ± 2.3 GPa and hardness of 1.18 ± 0.04 GPa were measured for Gr-removed Cu, and an elastic modulus of 119.3 ± 3.3 GPa and hardness of 1.14 ± 0.04 GPa were measured for Gr-coated Cu. Compared to Gr-removed Cu, there was an increase in elastic modulus of 1.7% and decrease in hardness of 3.2% caused by the graphene coating.

In ductile metals such as Cu, plastic pile-up generally occurs during nanoindentation, which is not taken into account in the Oliver–Pharr method.[24,31] By atomic force microscopy (AFM) scanning of residual indentation marks, as shown in Fig. 4(a), we found that the graphene coating affects the pile-up considerably. The pile-up height was measured as 22.3 (±2.08) nm for Gr-removed Cu and 18.9 (±3.06) nm for Gr-coated Cu, meaning that the graphene coating suppressed the pile-up. AFM scanning was carried out for at least 20 residual nanoindentation marks for each sample that were formed with reproducible nanoindentation force-depth curves. The ultra-stiff graphene is likely to suppress the upward stress that would otherwise introduce a pile-up in the vicinity of the indenter. Figure 4(b) shows the distribution of the von Mises stresses at the indentation depth of 100 nm in Gr-removed Cu and Gr-coated Cu, as simulated by FEA. The von Mises stress boundary of the Gr-coated Cu near the indenter are more restricted than that of Gr-removed Cu along the in-plane direction, whereas they distribute deeper along the loading direction, as indicated by the orange arrows in Fig. 4(b). As shown in the insets of Fig. 4(b), this difference in stress distribution results in pile-up heights of 2.30 nm for Gr-coated Cu and 9.23 nm for Gr-removed Cu—the same trend as for AFM measurements. True contact height h_{true} is given by $h_{true} = h_{max} - h_d + h_{pile\text{-}up}$, where h_{max} is the maximum indentation depth, h_d is the elastic deflection depth, and $h_{pile\text{-}up}$ is the pile-up height.[32–34] By this correction, using the pile-up heights as measured by AFM, an elastic modulus of 98.3 ± 2.7 GPa and hardness of 0.81 ± 0.05 GPa were calculated for Gr-removed Cu, and an elastic modulus of 103.3 ± 2.7 GPa and hardness of 0.82 ± 0.05 GPa were calculated for Gr-coated Cu. This means that the graphene coating enhanced the elastic modulus by 5% and does not significantly change hardness, even in the fully plastic contact region at an indentation depth of 100 nm. It is notable that variations of hardness and hardness by corrections for pile-up heights are not expected to depend on the indentation depth for the fully plastic contact region.[35]

We have demonstrated how a graphene layer coated on Cu affects the contact behavior during nanoindentations. In the initial elastic contact region, Gr-coated Cu showed stiffer loading than Gr-removed Cu, which could be attributed to the enhanced elastic modulus due to the ultra-high elastic modulus of graphene and

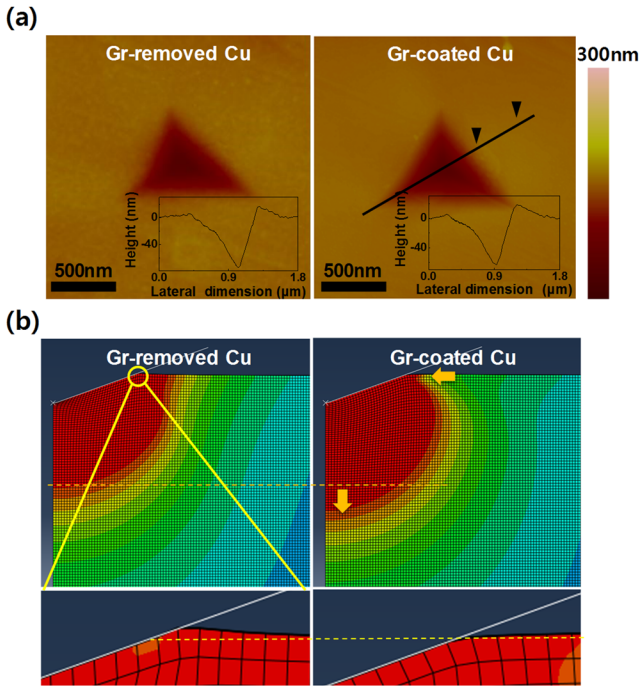

FIG. 4. (a) AFM images of residual indentation marks for graphene-removed Cu and graphene-coated Cu. (b) Distributions of von Mises stress in the loaded state analyzed by FEA. The insets show pile-up heights in the loaded state.

the introduction of compressive in-plane residual stresses in the Cu surface volume. The graphene coating affected the fully plastic contact behavior considerably by suppressing the pile-up around the indenter, despite there being just a 0.34 nm thickness of graphene. Compared to Gr-removed Cu, the stress distribution in Gr-coated Cu under the indenter showed a confined feature through FEA investigation, which coincides with the contact perimeter. The true contact area was modified using the pile-up height, which revealed that the Gr-coated Cu has a 5% enhanced elastic modulus compared to Gr-removed Cu at an indentation depth of 100 nm, while showing similar hardness.

This work was supported by the Institute for Basic Science (No. IBS-R019-D1), by the National Research Foundation of Korea (NRF) grant funded by the Ministry of Science, ICT and Future Planning (MSIP) (Grant No. NRF-2015R1A15A1037627), and by the Global Frontier R&D Program on Center for Multiscale Energy System funded by the National Research Foundation under the Ministry of Science, ICT and Future Planning, Korea (Grant No. 2012M3A6A7054855).

REFERENCES

[1] G. H. Lee, R. C. Cooper, S. J. An, S. Lee, A. van der Zande, N. Petrone, A. G. Hammerberg, C. Lee, B. Crawford, W. Oliver, J. W. Kysar, and J. Hone, Science **340**(6136), 1073–1076 (2013).
[2] C. Lee, X. Wei, J. W. Kysar, and J. Hone, Science **321**(5887), 385–388 (2008).
[3] A. A. Balandin, S. Ghosh, W. Bao, I. Calizo, D. Teweldebrhan, F. Miao, and C. N. Lau, Nano Lett. **8**(3), 902–907 (2008).
[4] M. Y. Han, B. Ozyilmaz, Y. Zhang, and P. Kim, Phys. Rev. Lett. **98**(20), 206805 (2007).
[5] I. N. Kholmanov, C. W. Magnuson, A. E. Aliev, H. Li, B. Zhang, J. W. Suk, L. L. Zhang, E. Peng, S. H. Mousavi, A. B. Khanikaev, R. Piner, G. Shvets, and R. S. Ruoff, Nano Lett. **12**(11), 5679–5683 (2012).
[6] Y. Kim, J. Lee, M. S. Yeom, J. W. Shin, H. Kim, Y. Cui, J. W. Kysar, J. Hone, Y. Jung, S. Jeon, and S. M. Han, Nat. Commun. **4**, 2114 (2013).
[7] S.-Y. Park, E.-J. Gwak, M. Huang, R. S. Ruoff, and J.-Y. Kim, Scr. Mater. **139**, 63–66 (2017).
[8] B. Wang, B. V. Cunning, S. Y. Park, M. Huang, J. Y. Kim, and R. S. Ruoff, ACS Nano **10**, 9794 (2016).
[9] M. Hammad, J. J. Adjizian, C. H. Sacré, B. Huet, J. C. Charlier, J. P. Raskin, and T. Pardoen, Carbon **122**, 446–450 (2017).
[10] A. Klemenz, L. Pastewka, S. G. Balakrishna, A. Caron, R. Bennewitz, and M. Moseler, Nano Lett. **14**(12), 7145–7152 (2014).
[11] C. Yan, K.-S. Kim, S.-K. Lee, S.-H. Bae, B. H. Hong, J.-H. Kim, H.-J. Lee, and J.-H. Ahn, ACS Nano **6**, 2096–2103 (2012).
[12] A. Klemenz, A. Gola, M. Moseler, and L. Pastewka, Appl. Phys. Lett. **112**, 061601 (2018).
[13] K. Shinohara, J. Mater. Sci. **28**, 5325–5329 (1993).
[14] X. Tan, J. Wu, K. Zhang, X. Peng, L. Sun, and J. Zhong, Appl. Phys. Lett. **102**, 071908 (2013).
[15] A. C. Ferrari, J. C. Meyer, V. Scardaci, C. Casiraghi, M. Lazzeri, F. Mauri, S. Piscanec, D. Jiang, K. S. Novoselov, S. Roth, and A. K. Geim, Phys. Rev. Lett. **97**(18), 187401 (2006).
[16] D. W. Kim, J. Lee, S. J. Kim, S. Jeon, and H.-T. Jung, J. Mater. Chem. C **1**(47), 7819 (2013).
[17] Z.-J. Wang, G. Weinberg, Q. Zhang, T. Lunkenbein, A. Klein-Hoffmann, M. Kurnatowska, M. Plodinec, Q. Li, L. Chi, R. Schloegl, and M.-G. Willinger, ACS Nano **9**, 1506–1519 (2015).
[18] J.-Y. Kim, J.-J. Lee, Y.-H. Lee, J.-i. Jang, and D. Kwon, J. Mater. Res. **21**(12), 2975–2978 (2011).
[19] J.-Y. Kim, S.-K. Kang, J.-J. Lee, J.-i. Jang, Y.-H. Lee, and D. Kwon, Acta Mater. **55**(10), 3555–3562 (2007).
[20] T.-H. Ahn, C.-S. Oh, K. Lee, E. P. George, and H. N. Han, J. Mater. Res. **27**(01), 39–44 (2011).
[21] K. L. Johnson and K. L. Johnson, *Contact Mechanics* (Cambridge University Press, 1987).
[22] A. Gouldstone, H.-J. Koh, K.-Y. Zeng, A. E. Giannakopoulos, and S. Suresh, Acta Mater. **48**, 2277–2295 (2000).
[23] S. Pathak, L. J. Riesterer, R. S. Kalidindi, and J. Michler, Appl. Phys. Lett. **105**, 161913 (2014).
[24] W. C. Oliver and G. M. Pharr, J. Mater. Res. **7**(6), 1564–1583 (1992).
[25] X. Mi, V. Meunier, N. Koratkar, and Y. Shi, Phys. Rev. B **85**(15), 155436 (2012).
[26] R. He, L. Zhao, N. Petrone, K. S. Kim, M. Roth, J. Hone, P. Kim, A. Pasupathy, and A. Pinczuk, Nano Lett. **12**(5), 2408–2413 (2012).
[27] S. Suresh and A. E. Giannakopoulos, Acta Mater. **46**, 5755–5767 (1998).
[28] K. Sun, W. Shen, and L. Ma, Comput. Mater. Sci. **81**, 226–232 (2014).
[29] M. S. Hu, Appl. Phys. Lett. **31**, 139 (1977).
[30] S. Suresh, T.-G. Nieh, and B. Choi, Scr. Mater. **41**(9), 951–957 (1999).
[31] W. C. Oliver and G. M. Pharr, J. Mater. Res. **19**(1), 3–20 (2011).
[32] S.-K. Kang, Y.-C. Kim, K.-H. Kim, J.-Y. Kim, and D. Kwon, Int. J. Plast. **49**, 1–15 (2013).
[33] J.-Y. Kim, B.-W. Lee, D. T. Read, and D. Kwon, Scr. Mater. **52**(5), 353–358 (2005).
[34] Y. Choi, H.-S. Lee, and D. Kwon, J. Mater. Res. **19**(11), 3307–3315 (2011).
[35] K. Kese and Z. C. Li, Scr. Mater. **55**(8), 699–702 (2006).